Nuclear Instruments and Methods in Physics Research A 806 (2016) 383–394

Contents lists available at ScienceDirect

Nuclear Instruments and Methods in Physics Research A

journal homepage: www.elsevier.com/locate/nima

Advances in Multi-Pixel Photon Counter technology: First characterization results

G. Bonanno [a,*], D. Marano [a], G. Romeo [a], S. Garozzo [a], A. Grillo [a], M.C. Timpanaro [a], O. Catalano [b], S. Giarrusso [b], D. Impiombato [b], G. La Rosa [b], G. Sottile [b]

[a] INAF, Osservatorio Astrofisico di Catania, Via S. Sofia 78, I-95123 Catania, Italy
[b] INAF, Istituto di Astrofisica Spaziale e Fisica cosmica di Palermo, Via U. La Malfa 153, I-90146 Palermo Italy

ARTICLE INFO

Article history:
Received 5 July 2015
Received in revised form
13 October 2015
Accepted 16 October 2015
Available online 25 October 2015

Keywords:
Silicon Photomultipliers
Multi-Pixel Photon Counters
Fill-factor enhancement
Low Cross-Talk
Photon Detection Efficiency
Electro-optical characterization

ABSTRACT

Due to the recent advances in silicon photomultiplier technology, new types of Silicon Photomultiplier (SiPM), also named Multi-Pixel Photon Counter (MPPC) detectors have become recently available, demonstrating superior performance in terms of their most important electrical and optical parameters. This paper presents the latest characterization results of the novel Low Cross-Talk (LCT) MPPC families from Hamamatsu, where a noticeable fill-factor enhancement and cross-talk reduction is achieved. In addition, the newly adopted resin coating has been proven to yield improved photon detection capabilities in the 280–320 nm spectral range, making the new LCT MPPCs particularly suitable for emerging applications like Cherenkov Telescope Array, and Astroparticle Physics.

1. Introduction

Silicon photomultipliers (SiPMs) are a contemporary highly-competitive class of solid-state photodetectors particularly suitable for a growing number of applications in many fields of high-energy physics, nuclear medicine, and astrophysics. Due to their unique features in terms of photon counting capabilities, low operating voltages, fast dynamic response, structural compactness, and insensitivity to magnetic fields, SiPMs have found widespread popularity in high-energy astrophysics [1–14], positron emission tomography systems for nuclear medicine [15–17], and cosmic-ray muon detection [18, 19].

The exceptional characteristics offered by most commercially available devices from the world's leading manufacturers result from new integration approaches and modern semiconductor fabrication technologies. Remarkable effort is presently being devoted by the SiPM producers to further improve the overall performance achieved by this class of devices [20–22]. Moreover, the growing popularity of SiPMs in the sensors community has led to a significant number of characterization studies and methodologies for investigating and quantifying the detector performance [23–34]. The rising number of perspective applications requiring optimal speed and single photon time resolution, along with the consequent demand for suitable integrated front-ends, have also provided research motivation for accurate analytical studies on the SiPM time response, exploring the physical processes contributing to the signal formation in the individual pixels, and allowing a detailed analytical description of the sensor [35–38].

This paper presents and discusses the characterization of a new class of recently available multi-pixel photon counter (MPPC) detectors from Hamamatsu Photonics, demonstrating the latest advances in the fabrication technology used by the manufacturer. Measurements are carried out at the INAF – Catania astrophysical Observatory Laboratory for Detectors (COLD).

2. New-generation Low Cross-Talk MPPCs

SiPM photon-counting ability may be seriously limited by the optical cross-talk effect, originated by correlated coincidences of two (or multiple) induced avalanches, affecting the linearity of the detector response and causing a significant excess noise contribution. Because it is impossible to determine the number of pixels that were fired by external photons, cross-talk may limit the photon-counting resolution of a SiPM device. The probability of optical cross-talk could be considered as one of the crucial performance parameters of a SiPM detector for ground-based gamma-ray astrophysics. Operating a SiPM at low overvoltages would significantly diminish cross-talk effects, but at the expense of degrading the photon-detection efficiency. Isolation trenches

* Corresponding author.
E-mail address: gbonanno@oact.inaf.it (G. Bonanno).

http://dx.doi.org/10.1016/j.nima.2015.10.064
0168-9002/

Table 1
Main physical features of the characterized MPPC detectors.

Device series	LCT1	LCT4			LCT5
Serial number	LCT-B/25	LCT4/2	LCT4/9	LCT4/20	LCT5/1
Cell pitch	50 μm	50 μm	75 μm	100 μm	50 μm
Device size	3×3 mm^2	3×3 mm^2	3×3 mm^2	3×3 mm^2	3×3 mm^2
Microcells	3600	3600	1600	900	3600
Surface coating	Epoxy resin	Silicone resin	Silicone resin	Silicone resin	Silicone resin
Fill-factor	61%	61%	73%	79%	74%
Breakdown[a]	55.00 V	50.92 V	51.10 V	52.31 V	52.5 V

[a] At room temperature (25 °C).

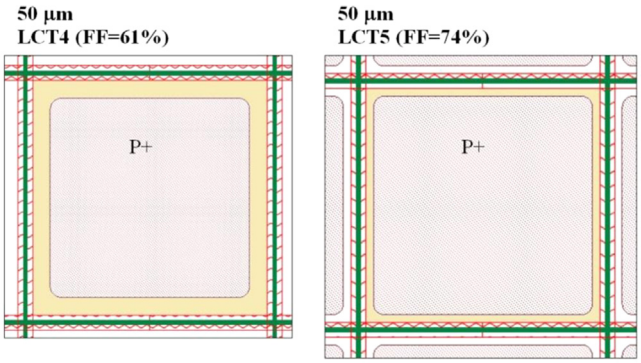

Fig. 1. Geometrical fill-factor enhancement from LCT4 to LCT5 50-μm MPPC devices: in this case, an improvement of 13% has been achieved (courtesy of Hamamatsu Photonics).

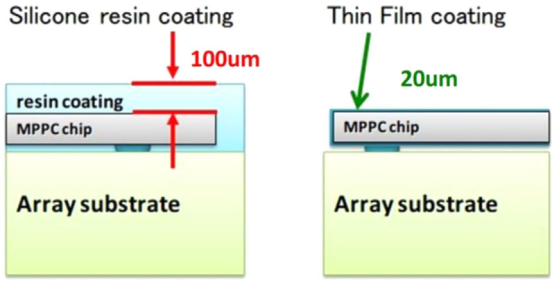

Fig. 2. Schematics of the silicone resin coating and thin film coating (courtesy of Hamamatsu Photonics).

around each pixel successfully reduce optical cross-talk. This technique has become a standard for this kind of photodetector; however, a non-negligible contribution to cross-talk can come from light reflected off the bottom surface of the silicon bulk, and thus, trenches would not be able to prevent this [21,39].

On the other hand, one of the main factors compromising the ability of a SiPM to generate an output signal from an incoming photon, i.e. its Photon Detection Efficiency (PDE), is its inherent geometrical inefficiency due to inactive regions between inner cells. The geometrical efficiency factor is defined as the ratio between the total active area of the SiPM cells and the overall device area, as a result of the gaps between the individual cells, and is solely determined by the detector topology. This parameter is commonly referred to as fill-factor.

To overcome such limitations, much effort has been put into technological progress and development of new types of detectors, and remarkable steps forward have been made in fill-factor enhancement and cross-talk reduction.

The characterized SiPM detectors presented in this paper are essentially the latest device series manufactured by Hamamatsu Photonics and identified by the definition of Low Cross-Talk (LCT)

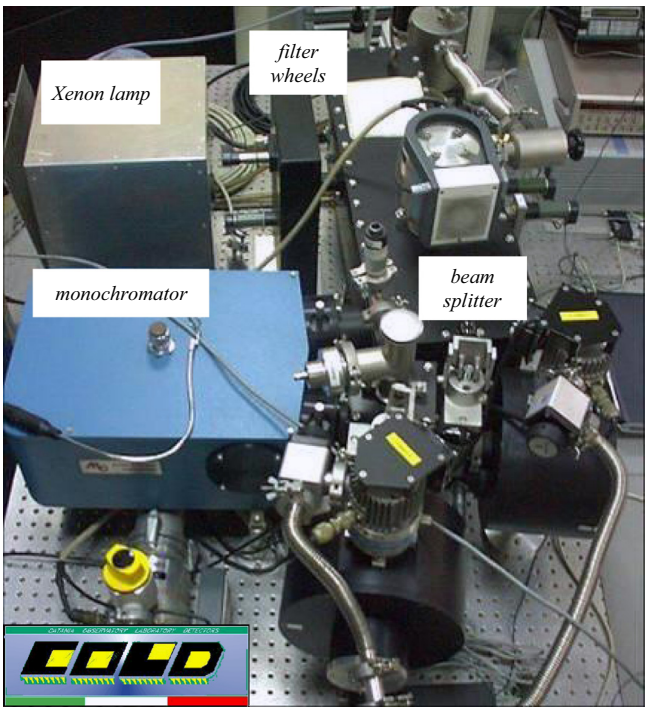

Fig. 3. COLD optical bench with the apparatus set-up used for SiPM tests and measurements.

MPPCs. They are prototype devices provided by the manufacturer to our laboratory for testing and evaluation purposes. Table 1 reports the main features of the characterized detectors. As a result of the recent advances in LCT technology, new generation MPPCs have been produced with improved characteristics and performance. New materials and processes have been adopted, aiming at achieving higher sensitivity and geometrical fill-factors.

The optical trench improvement of the LCT4 and LCT5 detectors compared to the prior MPPC series of the same family arises from new types of trenches enabling cross-talk reduction. On the other hand, the fill-factor improvement from the LCT4 to the LCT5 MPPC series results from a functional optimization of the physical structure and is pictorially sketched in Fig. 1 for the 50-μm devices. As shown, maximization of the active area (in gray) is accomplished for the LCT5 device.

In addition, epoxy resin coating, used for all previous MPPC devices tested in our labs [24–26], is adopted for the LCT1 series. However, compared to the epoxy resin coating, new thin film coating and silicone resin coating have been proven to show higher quantum efficiency in the near ultraviolet (NUV) spectral region. Both LCT4 and LCT5 series benefit from such technology development and address the challenge of high NUV sensitivity for applications like Imaging Atmospheric Cherenkov Telescopes [7].

The topological characteristics of the new thin film coating and silicone resin coating are schematically sketched in Fig. 2. Silicone resin coating advantages include robustness to mechanical shocks and easy handling (as for the epoxy resin coating); on the other hand, thin film coating presents a super smooth surface (minimum bending). LCT4 and LCT5 devices characterized in this work, as detailed in Table 1, are given a silicone resin coating; however, similar sensitivity improvements in the NUV region have been proven by the manufacturer to be achieved by the LCT MPPCs adopting thin film coating, which is definitely preferable to be used in MPPC arrays, due to its better ease of handling compared to the silicone resin coating.

3. Measurement set-up

The optical equipment used for SiPM measurements is shown in Fig. 3. The system uses a Xenon lamp as a light source, a wavelength selection system consisting of a set of band-pass filters and mirrors, a Czerny–Turner monochromator which selects the desired wavelength in the 130–1100 nm spectral range, a beam splitter for directing the monochromatic radiation through an optical lens, and an integrating sphere to which are attached a NIST-traceable reference photodiode and the SiPM detector under test. A detailed description of this facility can be found in [24–26, 33]; the system permits measurements of wavelengths down to the vacuum UV and is limited by the 116-nm cut-off due to the Magnesium Fluoride (MgF_2) focusing lenses and windows (when operated in vacuum conditions). In all previous SiPM characterizations, PDE measurements in the COLD laboratory were performed in the 350–950-nm spectral range. However, due to the improved optical features of the protective coating in the new series of LCT detectors discussed in this paper, the measurement range has been extended to include the spectral response in the 250–350-nm wavelength range, which is particularly important in applications like Cherenkov light detection, i.e., the Cherenkov Telescope Array (CTA) [5, 6].

The main element of the front-end electronics for SiPM characterization is the Cherenkov Imaging Telescope Integrated Read-Out Chip (CITIROC) [40–42], which is an advanced version of the Extended Analogue SiPM Integrated Read-Out Chip (EASIROC) [43–46], both produced by WEEROC. The modifications in CITIROC stem from INAF/IASF-Palermo and originated from the design of the camera of the ASTRI SST-2M telescopes [2,3]. CITIROC is a 32-channel fully-analog front-end ASIC specifically designed to directly interface SiPM detectors, working as a signal shaper, in which the input charge is integrated and the integral converted to an amplitude at the output of the ASIC. Each channel feeds two voltage-sensitive, AC-coupled, tunable-gain, and low-noise pre-amplifiers, one for high-gain (HG) and one for low-gain (LG) operation, in order to measure charges from 160 fC up to 320 pC, with a photoelectron-to-noise ratio of 10. Each pre-amplifier is followed by a tunable slow-shaper and a track-and-hold circuit to

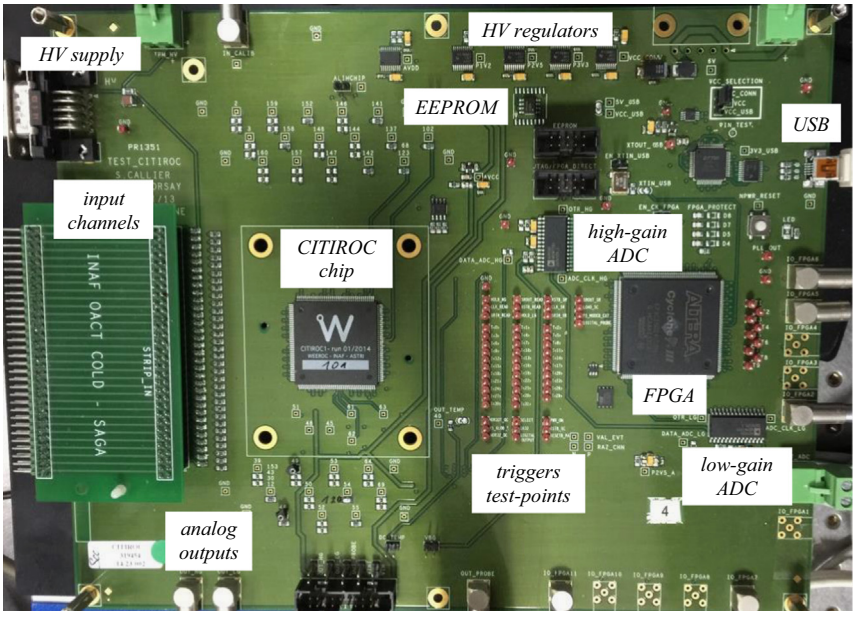

Fig. 4. CITIROC evaluation board used as front-end electronics to read out the SiPM signals. The main functional blocks are highlighted.

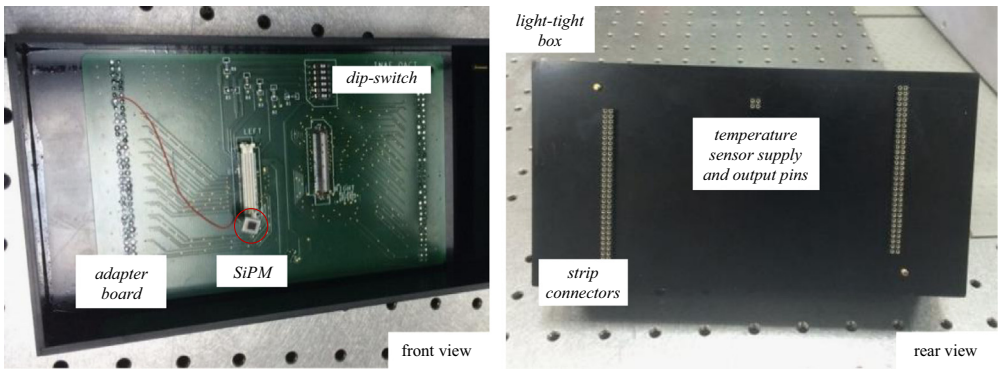

Fig. 5. Dedicated adapter board and mechanical support for interfacing the SiPM detector signals with the CITIROC evaluation board (left: front view, right: rear view).

catch the peak of the shaped signal. The sampled amplitude of all signals are read out by a pair of multiplexers (one for LG and one for HG) and subsequently digitized by an external ADC. A separate chain is additionally implemented to generate a trigger signal, composed of a fast shaper with a fixed shaping time of 15 ns, followed by two discriminators with independent threshold settings. Furthermore, each of the CITIROC channels is internally connected to an 8-bit Digital-to-Analog Converter (DAC) which finely adjusts the SiPMs bias voltage, allowing gain stabilization. Fig. 4 shows a photograph of the CITIROC evaluation board.

To provide a versatile interface between the SiPM terminals and the CITIROC evaluation board, a specific adapter board (visible in Fig. 5, front view) has been fabricated at the COLD laboratory, allowing to perform several functional tests and measurements for SiPM characterization. In particular, to easily interface the SiPM signals with the read-out evaluation board, two multi-pin connectors on the adapter board receive up to 64 signals, which are routed towards two 32-pin strip connectors located on the rear side of the adapter board. As a result, each of the strip connectors can couple 32 output signals to the input channels of the CITIROC evaluation board. Any SiPM detector to be tested and characterized can be connected to the adapter board by soldering its anode terminal to one of the connector pins of the board, and its cathode terminal to the strip connector, as shown in Fig. 5. A calibrated temperature sensor is attached to the detector under test inside the light-tight box. Moreover, a dip-switch in the adapter board can allow individual selection of the voltage signals for a maximum of 16 temperature sensors, providing 2^4 input digital selectors to an integrated analog multiplexer.

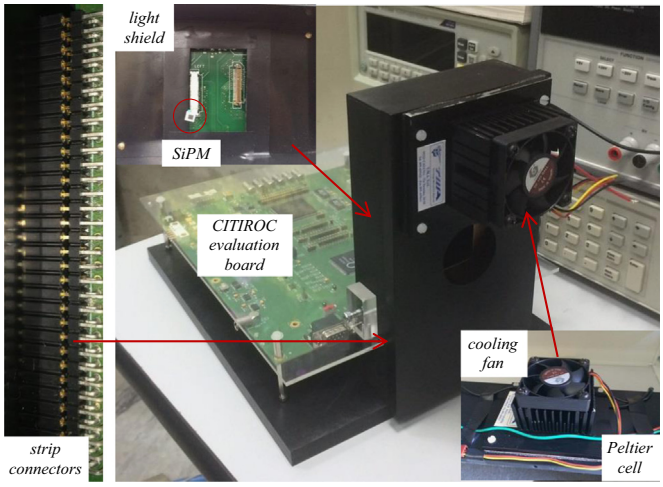

Fig. 6. Electronics apparatus set-up for SiPM tests and measurements.

An additional mechanical support has been set to house the adapter board with the SiPM detectors; in particular, the black light-tight box shown in Fig. 5 prevents accidental light exposure of the SiPM detectors. A light shield has been set on top of the adapter board in order to prevent light penetration through the back of the black-box, and helps to stabilize the temperature inside the box, avoiding heat exchange with outside air. The temperature control of the SiPM sensors is obtained through a dedicated thermoelectric cooling system based on a Peltier cell, whose hot side is cooled by a CPU fan. The entire cooling system is thermally calibrated and can reach temperatures down to 10 °C. The cool side of the Peltier cell is connected to an aluminum foil of sufficient thickness so as to penetrate inside the black box and approach to the inner SiPM package, so that temperature stabilization of the SiPM is achieved through convective air flow. Thermal calibration and control allows the selection of the desired temperature. The assembled electronics apparatus set-up is depicted in Fig. 6.

4. Experimental results

This section reports the experimental measurements carried out on all detectors of the LCT series in terms of the main MPPC performance parameters, i.e. gain, dark count rate, cross-talk and PDE.

4.1. Gain measurements

To evaluate the detector gain at a given temperature and for a specific range of operating voltages, charge amplitude histograms are produced while illuminating the SiPM detector with a light source of tunable intensity and duration. By computing the average spacing between subsequent charge peaks (in terms of ADC channels), and scaling for the constant ADC rate (charge/channel) and amplification factor, the SiPM gain is obtained for a fixed bias condition. A detailed description of the apparatus and the adopted technique can be found in [25]. The obtained gain data points as a function of the applied overvoltage *OV* at room temperature are reported in Fig. 7 for all characterized detectors.

It can be noted from the plot that the obtained MPPC gain for the 50-μm LCT1 and LCT4 detectors are similar (nearly 1.7×10^6 at $OV = 3.0$ V, and so forth), due to the same active area dimensions of the single cells, while the LCT5 MPPC of the same cell size results in a slightly greater gain (2.0×10^6 at $OV = 3.0$ V), in accordance with the achieved maximization of the active area in the LCT5 device series. On the other hand, as expected, the 75-μm and 100-

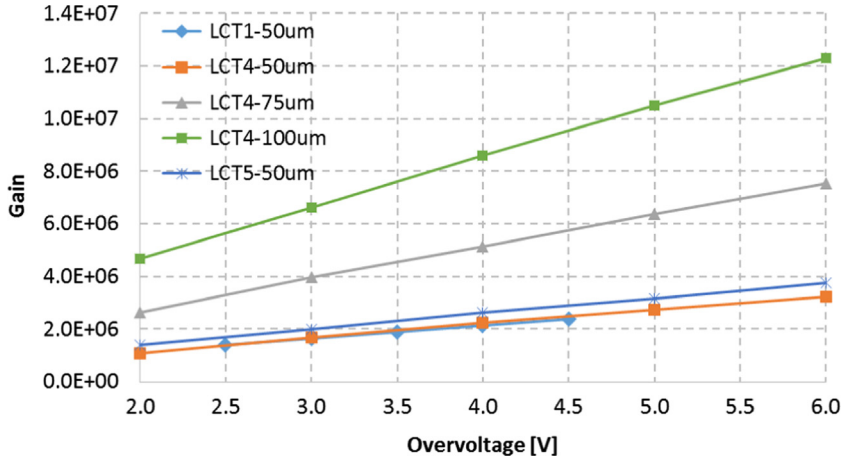

Fig. 7. Gain measurements of the characterized LCT detectors as a function of the applied overvoltage at room temperature.

μm LCT4 counterparts exhibit higher gain (4.0×10^6 and 6.6×10^6 at $OV = 3.0$ V, respectively) owing to the greater dimensions, and hence capacitance, of the single cells.

The slopes of the linear fits in the above plots allow for an estimation of the global terminal capacitance of the LCT MPPCs, as described in [25]. The assessed values for all LCT4 devices are found to be approximately the same (about 310 pF), since larger active area resulting from increased cell size implies a reduced number of cells for equal global dimensions (3×3 mm^2). A higher value of 340 pF is estimated for the LCT5 device, which is consistent with the slightly larger sensitive area compared to the LCT4 counterparts.

4.2. Staircase measurements: dark count rate and cross-talk

To measure the thermal noise rate plots, the SiPM dark signal is amplified and fed into a discriminator module, generating a logic output pulse each time a dark pulse crosses a predefined voltage

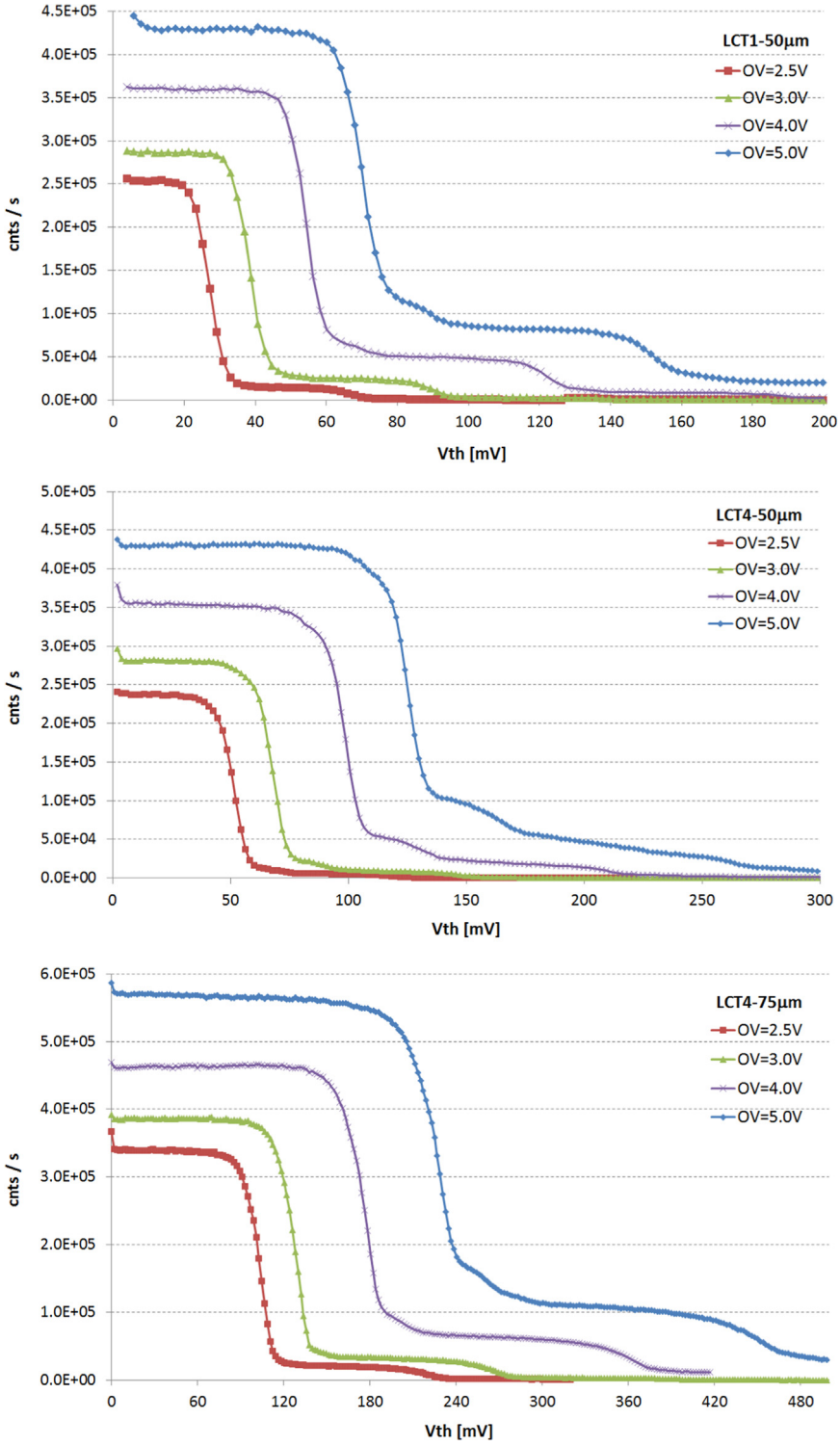

Fig. 8. Staircase measurements of the characterized LCT detectors as a function of the discriminator threshold at room temperature.

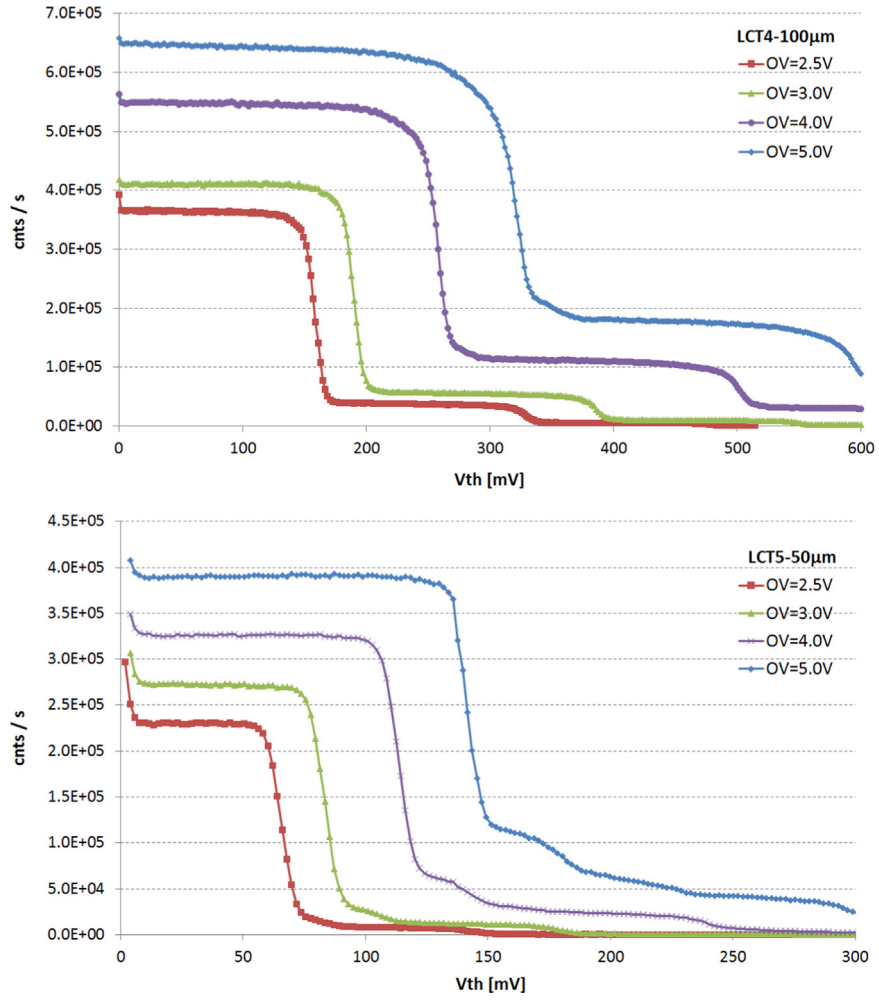

Fig. 8. (*continued*)

level, allowing to select the appropriate threshold to be used for the PDE measurements and evaluate the cross-talk contribution.

The dark count rate (DCR) is one of the main parameters of SiPM detectors. It is defined as the number of avalanche pulses produced by hot carriers simulating the detection of single photons at a certain bias voltage.

For a threshold above the electronics noise and below the photo-electron (pe) amplitude, all thermally generated avalanches are counted, including tunnel assisted charge carrier generation, afterpulsing and indirect optical cross-talk (extra-charge noise). By comparing the measured event rates above 1-pe threshold with the total dark rate, the cross-talk probability is estimated.

SiPM optical cross-talk, as reported in the literature, is evaluated as the ratio of the DCR at 1.5pe with respect to that at 0.5pe [1,24–26]. This approach is based on the assumption that the probability of triggering two uncorrelated avalanches at the same time is negligible.

Fig. 8 shows the DCR curves (also known as staircase functions) for all characterized LCT detectors as a function of the discriminator threshold and for different overvoltage values. Extra-charge noise effects at overvoltages higher than 3 V result in a peculiar feature of the staircase curves between the first edge and the second plateau.

The functional dependency of the dark-count rate and cross-talk on the operating voltage has also been investigated. Cross-talk and DCR measurement results for the analyzed detectors with various operating voltages are illustrated in Fig. 9 at $T=25$ °C, where the rising trends of both parameters are observed.

The improvement in cross-talk reduction in the LCT4 and LCT5 detectors compared to the older LCT1 type is evident. For instance, at $OV=4.0$ V a ~13% cross-talk is found for the 50-µm LCT1 device, while a ~5% and a ~6% cross-talk are obtained for the 50-µm LCT4 and LCT5 MPPCs, respectively. As expected, for equal overvoltage values, the 50-µm LCT5 detector results in a slightly higher cross-talk probability with respect to the LCT4 MPPC of the same cell size, due to its increased gain.

4.3. Photon detection efficiency measurements

SiPM absolute PDE measurements are carried out based on the photon counting method [24–26], by which the number of pulses per unit time in monochromatic light conditions are compared to the light level recorded by a reference NIST photodetector at the same time and for several wavelengths.

It should be mentioned that optical cross-talk is not accounted for in the adopted photon counting technique for determining the detector PDE, as a 0.5-pe threshold is applied to all triggered pulses, such that simultaneous pulses are always measured as a single pulse. However, the obtained PDE results are not immune to indirect cross-talk and afterpulsing, and therefore are slightly overestimated. Afterpulsing probability is stated in the manufacturer's specifications to be 0.1% in the 100–500 ns range, and SiPM extra-charge noise is typically on the order of 1–2% [39]. Also, the involved photon flux is kept sufficiently low, in order to minimize the probability that two or more photons impinge on

the given cell at the same time, which would lead to a lower count rate and, consequently, to a lower PDE.

PDE measurements in the 250–1000 nm spectral range of the LCT1 detector are shown in Fig. 10 as a function of wavelength and for different overvoltage values. PDE results for the three LCT4 devices are shown in Figs. 11–13, while those for the LCT5 MPPC are illustrated in Fig. 14. As expected, an increase in PDE is obtained for higher overvoltage values.

To better highlight the photo-detection capabilities of the new LCT families over the older LCT1 series in the UV spectral region, the PDE curves of the 50-μm LCT1 and LCT4 detectors at $OV = 3.0$ V are merged together in Fig. 15, along with the typical Cherenkov light emission spectrum from extended air showers [7]. Inspecting the figure, it clearly appears that in the 300–360-nm wavelength range a noticeable PDE enhancement of the new LCT family is achieved (dotted rectangle); in particular, at 320 nm a four-time increase in PDE is attained.

For the same 3-V overvoltage, PDE curves of all characterized MPPCs of the new LCT4 and LCT5 families are compared in Fig. 16. As expected, for the LCT4 devices the PDE scales with the cell pitch, reaching ~42% peak value for the 100-μm MPPC. It can be also observed a PDE improvement of the newer LCT5 detector with respect to the same LCT4 counterpart of the same 50-μm cell size, confirming the achieved maximization of the active area; in particular, a photon detection improvement from ~16% to ~22% is observed for the LCT5 MPPC at 320 nm, and a similar PDE enhancement is seen around the peak values (480 nm). However, only part of the measured increase in PDE below ~450 nm is due to the fill-factor enhancement, and the additional increase is due to the improved silicone resin coating of the newer LCT5 device, that has been demonstrated to show higher sensitivity below ~450 nm compared to the coating used in the LCT4 MPPC.

PDE values are increased for higher overvoltages approaching a peak of 45% for the 100-μm LCT4 MPPC and 42% for the 50-μm LCT5 MPPC at $OV = 5.0$ V.

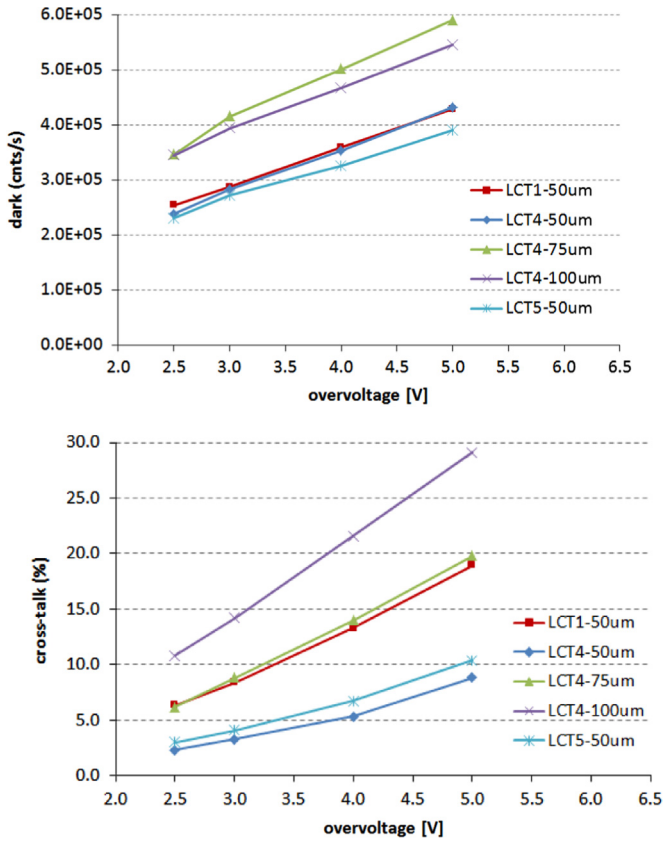

Fig. 9. DCR and cross-talk measurements of the characterized LCT detectors as a function of the applied overvoltage at room temperature.

4.4. Global comparisons and discussion

To achieve a global comparison among the tested MPPC detectors in terms of their most significant performance parameters, and to help choose the optimal operating condition for a specific device, Figs. 17 and 18 depict the PDE at a wavelength of 450 nm and the cross-talk measurements as a function of the applied overvoltage, respectively for the characterized 50-μm MPPCs and for the analyzed LCT4 MPPCs of different cell sizes.

As shown, the noticeable cross-talk reduction and PDE enhancement of the newer LCT5 device is apparent compared to the older LCT1 MPPC. On the other hand, greater cell size infers higher PDE capabilities at the expense of a slight increase in cross-talk.

Fig. 19 illustrates the PDE measurements of all characterized detectors at the same 450 nm wavelength as a function of cross-talk. Each single data point in the plot implicitly reflects the PDE and cross-talk functional dependency on the overvoltage, as

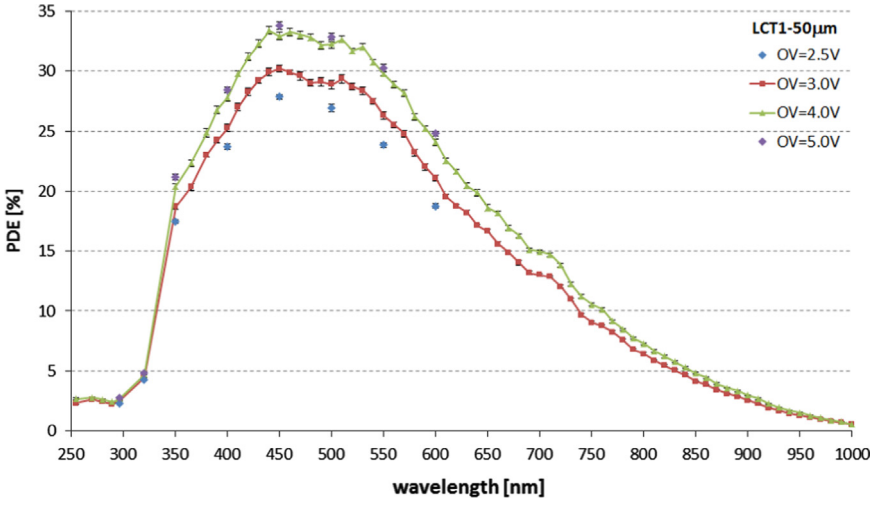

Fig. 10. PDE measurements of the characterized LCT1 50-μm detector at various overvoltages. The PDE measurements at 3-V and 4-V overvoltage are carried out in the 250–1000 nm spectral range in steps of 10 nm, while for the other overvoltages only eight points are shown.

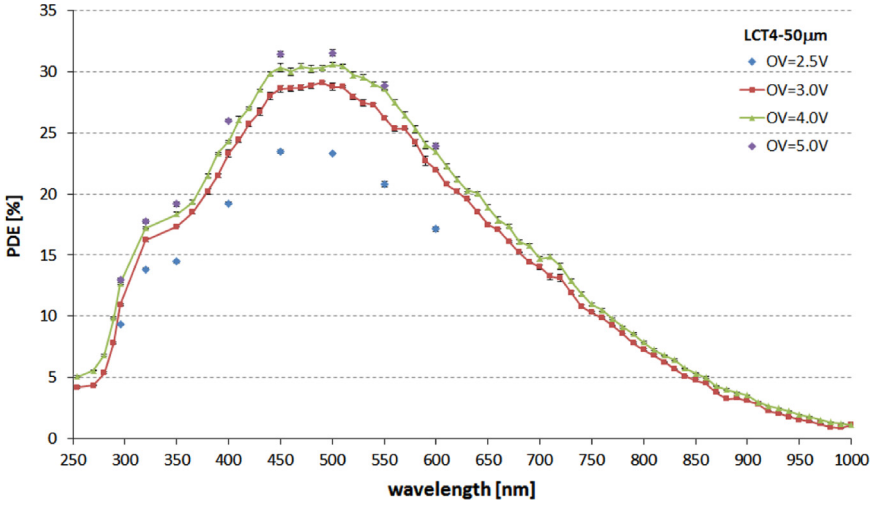

Fig. 11. PDE measurements of the characterized LCT4 50-µm detector as a function of wavelength at various overvoltages. The PDE measurements at 3-V and 4-V overvoltage are carried out in the 250–1000 nm spectral range in steps of 10 nm, while for the other overvoltages only eight points are shown.

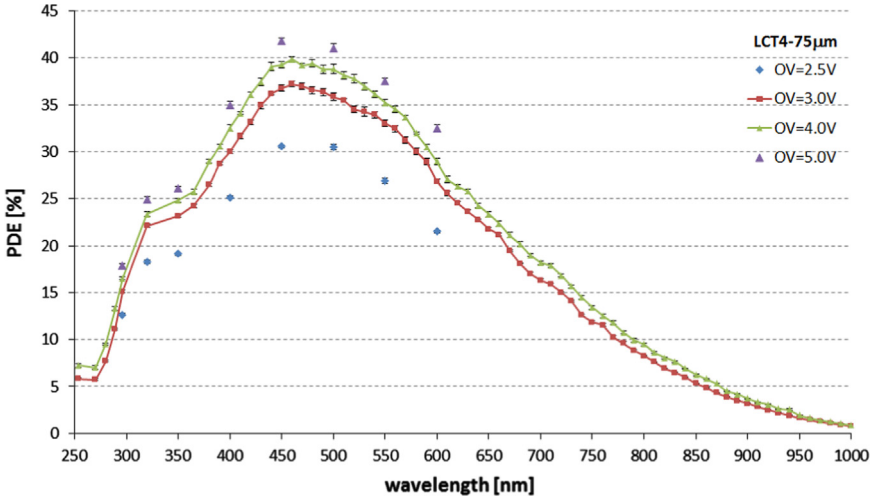

Fig. 12. PDE measurements of the characterized LCT4 75-µm detector as a function of wavelength at various overvoltages. The PDE measurements at 3-V and 4-V overvoltage are carried out in the 250–1000 nm spectral range in steps of 10 nm, while for the other overvoltages only eight points are shown.

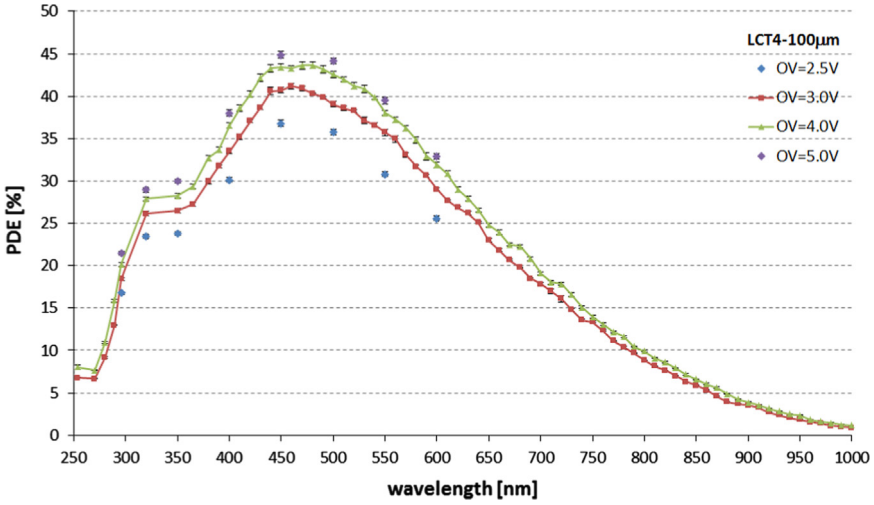

Fig. 13. PDE measurements of the characterized LCT4 100-µm detector as a function of wavelength at various overvoltages. The PDE measurements at 3-V and 4-V overvoltage are carried out in the 250–1000 nm spectral range in steps of 10 nm, while for the other overvoltages only eight points are shown.

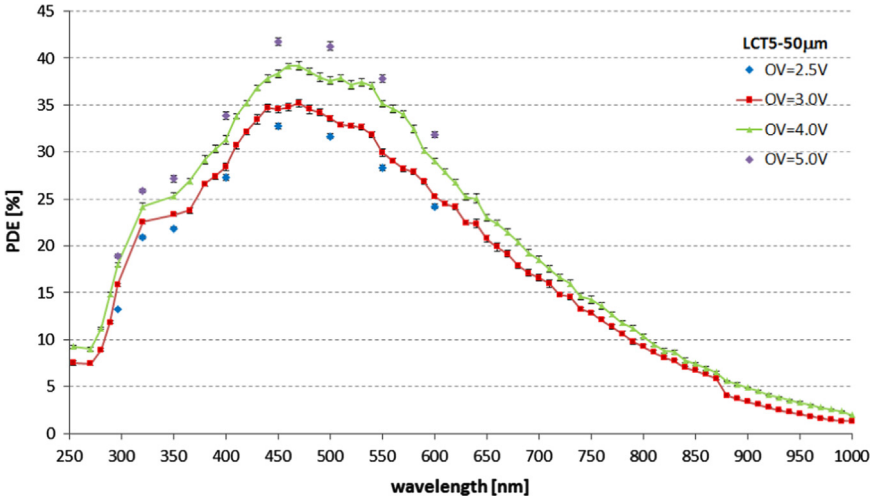

Fig. 14. PDE measurements of the characterized LCT5 50-μm detector as a function of wavelength at various overvoltages. The PDE measurements at 3-V and 4-V overvoltage are carried out in the 250–1000 nm spectral range in steps of 10 nm, while for the other overvoltages only eight points are shown.

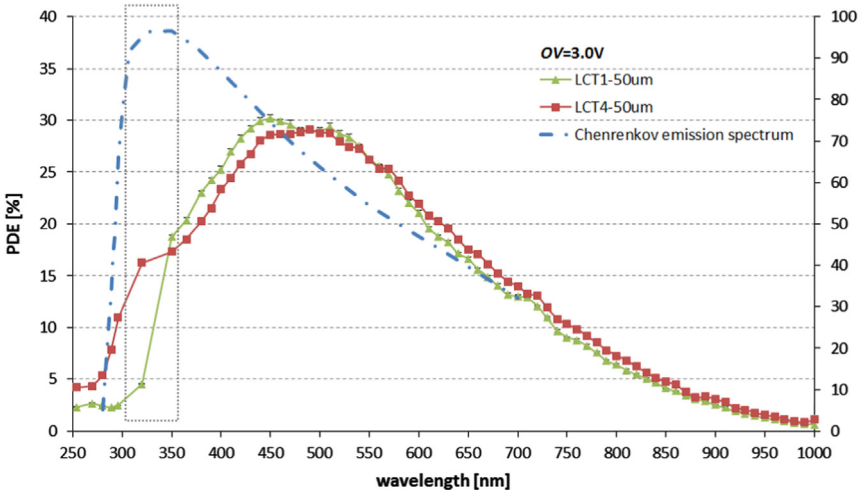

Fig. 15. PDE measurements comparison of the 50-μm cell size LCT1 and LCT4 detectors as a function of wavelength at $OV=3.0$ V, showing the UV sensitivity improvement of the new device family over the older LCT1 series. The right y-axis represents the Cherenkov light emission spectrum from extended air showers, expressed in arbitrary units.

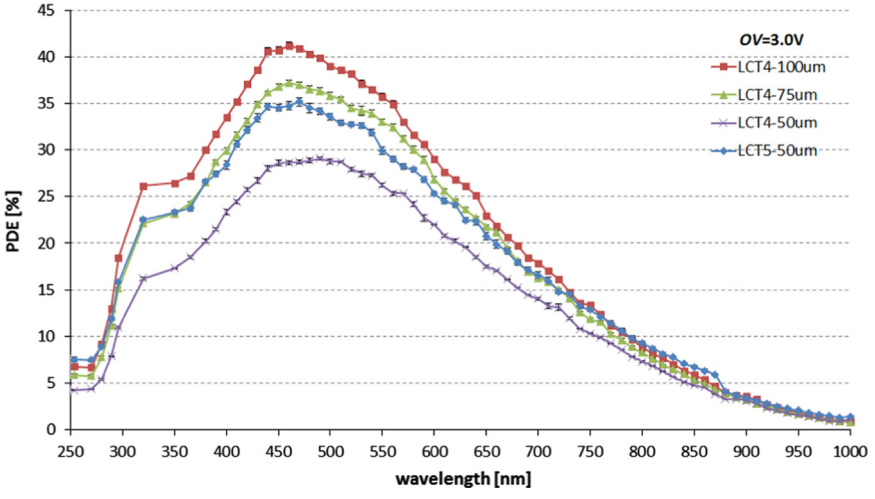

Fig. 16. PDE measurements comparison of the LCT4 and LCT5 detectors as a function of wavelength at $OV=3.0$ V. The improved detection capabilities of the new LCT5 family over the LCT4 series is apparent for the same cell-size.

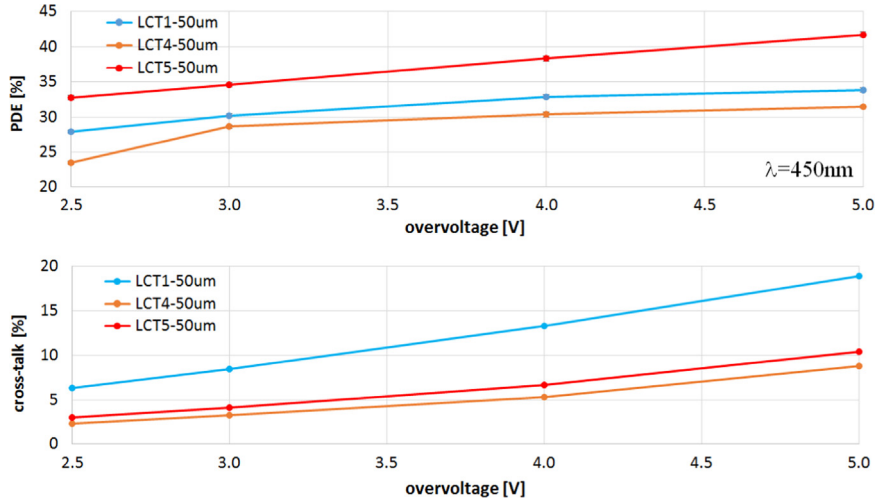

Fig. 17. PDE (450 nm) and cross-talk comparison of the 50-μm LCT detectors as a function of the applied overvoltage.

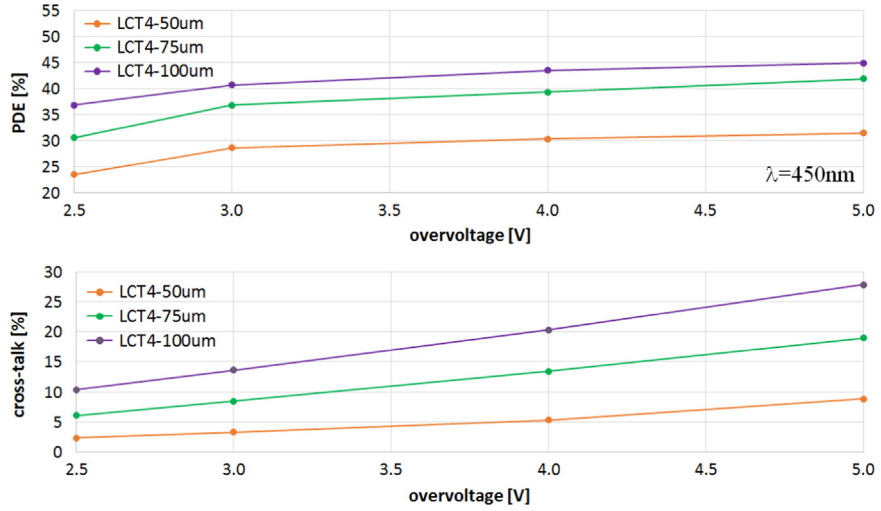

Fig. 18. PDE (450 nm) and cross-talk comparison of the LCT4 detectors as a function of the applied overvoltage.

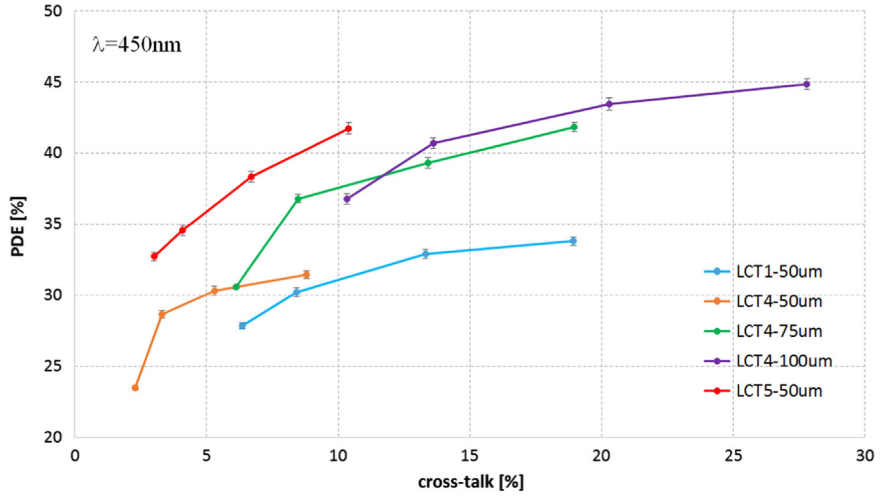

Fig. 19. PDE (450 nm) and cross-talk comparison of the LCT detectors as a function of the applied overvoltage.

Table 2
Measurement results for the main parameters of the characterized LCT detectors[a].

Device series			LCT1	LCT4			LCT5
Cell pitch			50 μm	50 μm	75 μm	100 μm	50 μm
Fill-factor			61%	61%	73%	79%	74%
Gain	$OV=3.0$ V		1.66×10^6	1.69×10^6	3.96×10^6	6.61×10^6	2.01×10^6
	$OV=4.0$ V		2.15×10^6	2.24×10^6	5.12×10^6	8.61×10^6	2.63×10^6
DCR (kHz)	$OV=3.0$ V		287	282	415	394	272
	$OV=4.0$ V		360	353	502	468	326
X-Talk (%)	$OV=3.0$ V		8.4	3.3	8.8	14.2	4.1
	$OV=4.0$ V		13.3	5.3	14.0	21.6	6.7
PDE (%)	$\lambda=320$ nm	$OV=3.0$ V	4.50	16.24	22.14	26.16	22.54
		$OV=4.0$ V	4.73	17.21	23.38	27.89	24.18
	$\lambda=450$ nm	$OV=3.0$ V	30.21	28.63	36.80	40.71	34.56
		$OV=4.0$ V	32.91	30.33	39.29	43.45	38.33

[a] At room temperature (25 °C).

higher *x*-axis values for the same detector refer to increased operating voltages.

Again, the superior overall performance of the LCT5 device is evident, since it provides the best compromise between high PDE and low cross-talk (Table 2).

Table 1 summarizes the most significant MPPC performance parameter results for all tested devices.

5. Conclusions and future work

In this paper, measurement results of a newly available class of MPPC detectors are reported and discussed. The newer LCT MPPCs achieve a significant cross-talk reduction, due to optical trench improvements, and much higher photon detection efficiency, due to geometrical fill-factor enhancement. In addition, novel types of coating allow for an improved photon-detection capability in the NUV spectral region, making these newer MPPCs particularly suitable for new and challenging applications demanding higher photon detection capabilities in the 300–360 nm wavelength range.

A new LCT5 sample with a 75-μm pixel size has already been produced by the manufacturer, and future measurements are foreseen at short term. Higher fill-factor and, in turn, PDE values are expected compared to the 50-μm LCT5 device characterized in this paper.

Acknowledgments

This work was supported in part by the ASTRI Flagship Project, financed by the Italian Ministry of Education, University, and Research (MIUR) and led by the Italian National Institute for Astrophysics (INAF). We acknowledge partial support by the MIUR Bando Prin 2009 and Teche.it 2014 Special Grants.

This paper has gone through internal review by the CTA Consortium, whose referees are gratefully acknowledged for their valuable comments and suggestions.

References

[1] D. Marano, et al., Nuclear Instruments and Methods in Physics Research A 768 (2014) 32.
[2] G. Pareschi et al., The dual-mirror Small Size Telescope for the Cherenkov Telescope Array, in: Proceedings of the 33rd International Cosmic Ray Conference (ICRC '13), Rio De Janeiro, Brazil, 2013.
[3] O. Catalano et al., The camera of the ASTRI SST-2M prototype for the Cherenkov Telescope Array, in: Proceedings of SPIE '14, Ground-based and Airborne Instrumentation for Astronomy V, vol. 91470D, Montreal, Canada, 2014.
[4] S. Vercellone et al., The ASTRI miny-array science case, In: Proceedings of the 33rd International Cosmic Ray Conference (ICRC 2013), Rio De Janeiro, Brazil, July 2013.
[5] O. Catalano et al., The ASTRI SST-2M prototype: camera and electronics, In: Proceedings of the 33rd International Cosmic Ray Conference (ICRC '13), Rio de Janeiro, 2013.
[6] B.S. Acharya, et al., Astroparticle Physics 43 (2013) 3.
[7] A. Bouvier et al., Photosensor characterization for the cherenkov telescope array: silicon photomultiplier versus multi-anode photomultiplier tube, In: Proceedings of SPIE, Hard X-Ray, Gamma-Ray, and Neutron Detector Physics XV, vol. 8852, San Diego, USA, 2013.
[8] H. Anderhub, et al., Journal of Instrumentation 4 (2009) P10010.
[9] H. Anderhub, et al., Journal of Instrumentation 8 (2013) P06008.
[10] A. Biland, et al., Journal of Instrumentation 9 (2014) P10012.
[11] D. Mazin et al., Towards SiPM camera for current and future generations of Cherenkov telescopes, In: Proceedings of the 33rd International Cosmic Ray Conference (ICRC '13), Rio De Janeiro, Brazil, 2013.
[12] A. Biland, et al., Nuclear Instruments and Methods in Physics Research A 595 (1) (2008) 165.
[13] N. Otte, et al., Nuclear Physics B – Proceedings Supplements 150 (2006) 144.
[14] G. Sottile, et al., Nuclear Physics B – Proceedings Supplements 239 (2013) 258.
[15] P. Buzhan, et al., Nuclear Instruments and Methods in Physics Research A 504 (2003) 48.
[16] S. Siefert, et al., Proc. IEEE Nuclear Science Symposium Conference Records (2009) 2329.
[17] N. Otte, et al., Nuclear Physics B – Proceedings Supplements 150 (2006) 417.
[18] P. La Rocca, et al., Nuclear Instruments and Methods in Physics Research A 787 (2015) 236.
[19] F. Riggi, Nuclear Instruments and Methods in Physics Research A 764 (2014) 142.
[20] C. Piemonte, et al., IEEE Transactions on Nuclear Science NS54 (1) (2007) 236.
[21] B. Dolgoshein, et al., Nuclear Instruments and Methods in Physics Research A 695 (2012) 40.
[22] C. Jendrysik, et al., Nuclear Instruments and Methods in Physics Research A 718 (2013) 262.
[23] V. Boccone et al., Characterization of new hexagonal large-area geiger avalanche photodiodes, In: Proceedings of the IEEE 3rd International Conference on Advancements in Nuclear Instrumentation Measurement Methods and their Applications (ANIMMA), 2013, pp. 1–6.
[24] G. Bonanno, et al., IEEE Sensors Journal 14 (10) (2014) 3567.
[25] G. Bonanno, et al., IEEE Sensors Journal 14 (10) (2014) 3557.
[26] G. Bonanno, et al., Nuclear Instruments and Methods in Physics Research A 610 (2009) 93.
[27] P. Eckert, et al., Nuclear Instruments and Methods in Physics Research A 620 (1) (2010) 217.
[28] S.K. Yang, et al., Optics Express 22 (1) (2014) 716.
[29] O. Soto, et al., Nuclear Instruments and Methods in Physics Research A 732 (2013) 431.
[30] K. Doroud, et al., Nuclear Instruments and Methods in Physics Research A 753 (2014) 149.
[31] A. Vacherect, et al., Nuclear Instruments and Methods in Physics Research A 656 (1) (2011) 69.
[32] P. Buzhan, et al., Nuclear Instruments and Methods in Physics Research A 610 (2009) 131.
[33] G. Bonanno et al., Geiger Avalanche Photodiodes (G-APDs) and Their Characterization, Photodiodes, ISBN: 978-953-307-530-3, InTech, World Activities in 2011.
[34] D. Impiombato, et al., Journal of Instrumentation 9 (2014) C02015.
[35] D. Marano, et al., IEEE Sensors Journal 14 (8) (2014) 2749.
[36] D. Marano, et al., IEEE Transactions on Nuclear Science NS61 (1) (2014) 23.
[37] D. Marano, et al., Nuclear Instruments and Methods in Physics Research A 726 (2013) 1.

[38] S. Vinogradov, et al., Nuclear Instruments and Methods in Physics Research A 787 (2015) 148.
[39] I. Rech, et al., Optics Express 16 (12) (2008) 8381.
[40] J. Fleury, et al., Journal of Instrumentation 9 (1) (2014).
[41] D. Marano, et al., International Journal of Circuits, Systems and Signal Processing 8 (2014) 274.
[42] D. Impiombato, et al., Nuclear Instruments and Methods in Physics Research A 794 (2015) 185.
[43] S. Callier et al., EASIROC, An easy & versatile readout device for SiPM, In: Proceedings of TIPP, 2001.
[44] D. Marano, et al., International Journal of Modelling and Simulations 34 (4) (2015) 1–12.
[45] D. Impiombato, et al., Nuclear Instruments and Methods in Physics Research A 729 (2013) 484.
[46] D. Impiombato, et al., Nuclear Physics B-Proceedings Supplements 239 (2013) 254.